Applied Catalysis A: General 382 (2010) 1–9

Contents lists available at ScienceDirect

Applied Catalysis A: General

journal homepage: www.elsevier.com/locate/apcata

Quantitative study of catalytic activity and catalytic deactivation of Fe–Co/Al_2O_3 catalysts for multi-walled carbon nanotube synthesis by the CCVD process

Sophie L. Pirard [a,*], Georges Heyen [b], Jean-Paul Pirard [a]

[a] Laboratoire de Génie Chimique, B6a, Université de Liège, B-4000 Liège, Belgium
[b] Laboratoire d'Analyse et de Synthèse des Systèmes Chimiques, B6a, Université de Liège, B-4000 Liège, Belgium

ARTICLE INFO

Article history:
Received 10 February 2010
Received in revised form 30 March 2010
Accepted 30 March 2010

Keywords:
Carbon nanotubes
Catalytic deactivation
Modeling

ABSTRACT

The catalytic deactivation during multi-walled carbon nanotube (MWNT) synthesis by the CCVD process and the influence of hydrogen on it were quantified. Initial specific reaction rate, relative specific productivity and catalytic deactivation were studied. Carbon source was ethylene, and a bimetallic iron–cobalt catalyst supported on alumina was used. The catalytic deactivation was modeled by a decreasing hyperbolic law, reflecting the progressive accumulation of amorphous carbon on active sites. While the initial specific reaction rate was found not to be influenced by hydrogen, catalytic deactivation was found to be modified in the presence of hydrogen, which delayed and slowed down the deactivation by avoiding amorphous carbon deposition, thus leading to a greater relative specific productivity of carbon nanotubes.

1. Introduction

Carbon nanotubes consist of a variable number of graphene sheets rolled coaxially into a cylinder of nanometric diameter. After their discovery, nanotubes were found to possess many interesting properties and potential applications [1,2], which gave a strong impetus to the research devoted to understanding and improving their production. Among the many different routes leading to single-walled (SWNT) and multi-walled carbon nanotube (MWNT) production, the catalytic chemical vapor deposition (CCVD) process, consisting in this study in the decomposition of a hydrocarbon vapor into carbon and hydrogen on a catalytic surface at temperature varying usually from 600 °C to 1000 °C, seems to be the easiest way to scale up towards an economically viable production and a high yield [3]. Large scale reactors using the CCVD process to produce carbon nanotubes by metric tons are already running, using a fluidized bed reactor [4–8] or an inclined mobile-bed rotating reactor [9–12]. The inclined mobile-bed rotating reactor seems to be one of the most appropriate technologies because the kinetics of carbon nanotube synthesis by hydrocarbon decomposition is quite slow, and because the ratio between the volume of the product and the volume of the catalyst is very large, larger than 50 [10]. Because the CCVD process seems to be the most suitable method for producing large scale carbon nanotubes, research on new effective catalysts is essential. Catalysts used in the CCVD process for the synthesis of carbon nanotubes are usually iron, cobalt, or nickel-supported catalysts prepared by impregnation, co-precipitation or the sol–gel process [13]. The sol–gel process seems to be a very appropriate way to synthesize catalyst supports because it yields high surface area supports with high porosity, properties that facilitate the high dispersion of metal particles. The choice of the supporting material such as Al_2O_3, SiO_2, or MgO, has been found to be critical. The aluminum oxide catalyst support is generally used because the purification process is simplified [13,14].

There has been recent progress in understanding the growth mechanism for the CCVD process [15–17]. The growth mechanism would first consist of the adsorption and the decomposition of the hydrocarbon gas, then of the dissolution of carbon atoms in metal nanoparticles. Following this, the precipitation of carbon from the saturated metal particle would lead to the formation of tubular carbon solids, which are in a low energy form. If the growth mechanism of carbon nanotube synthesis has made the object of many researches, the mechanism of catalytic deactivation during carbon nanotube synthesis remains an open question. The literature exhibits very few researches on deactivation of catalysts for carbon nanotube synthesis, even in a qualitative way. The catalytic deactivation is said to be due to the formation of amorphous carbon on the catalytic surface, avoiding the reactional gases to reach active sites [18]. The only quantitative study deals with a computational fluid dynamics model to predict the yield of MWNTs produced by the CCVD process in a reactor using xylene as precursor and iron particles as catalyst [19]. Using the experimentally obtained exhaust gas concentrations, inverse calculations were conducted to determine apparent rate constants of the catalytic surface reactions. The

* Corresponding author. Fax: +32 4366 3545.
E-mail address: Sophie.Pirard@ulg.ac.be (S.L. Pirard).

0926-860X/$ – see front matter © 2010 Elsevier B.V. All rights reserved.
doi:10.1016/j.apcata.2010.03.064

Nomenclature

a	first parameter of catalytic deactivation (s)
A_i	preexponential factor of the kinetic rate constant of elementary step i ($mol_{C_2H_4}\ s^{-1}\ g^{-1}_{catalyst}$)
b	second parameter of catalytic deactivation (–)
C_P	poison concentration ($mol\ l^{-1}$)
d	third parameter of catalytic deactivation (s^{-1})
E_i	activation energy of elementary step i ($kJ\ mol^{-1}$)
ΔH°	standard ethylene adsorption enthalpy ($kJ\ mol^{-1}$)
k	kinetic rate constant ($mol_{C_2H_4}\ s^{-1}\ g^{-1}_{catalyst}$)
k_i	kinetic rate constant of elementary step i ($mol_{C_2H_4}\ s^{-1}\ g^{-1}_{catalyst}$)
K	ethylene adsorption constant (atm^{-1})
l_i	number of experiments performed at temperature i
$\tilde{m}$	relative mass of active catalyst (–)
$m_{catalyst}$	mass of catalyst ($g_{catalyst}$)
m_{CNTs}	mass of carbon nanotubes (g_C)
n_i	size of sample i
$P_{C_2H_4}$	ethylene partial pressure (atm)
P_{H_2}	hydrogen partial pressure (atm)
P_{He}	helium partial pressure (atm)
r_0	initial specific reaction rate ($mol_{C_2H_4}\ s^{-1}\ g^{-1}_{catalyst}$)
R	gas constant ($J\ mol^{-1}\ K^{-1}$)
s_e^2	experimental variance
s_i^2	variance of sample i
S	objective function
ΔS°	standard ethylene adsorption entropy ($J\ mol^{-1}\ K^{-1}$)
t	time (s) tabulated variable of the statistical Student's t-test (–)
t_{exp}	experimental t variable of the statistical Student's t-test (–)
T	temperature (K or °C)
Y	specific productivity ($g_C\ g^{-1}{}_{catalyst}$)
Y_{max}	maximal specific productivity ($g_C\ g^{-1}{}_{catalyst}$)
Y_{ij}	experimental value of the dependent variable corresponding to temperature i and experiment j (initial specific reaction rate ($mol_{C_2H_4}\ s^{-1}\ g^{-1}_{catalyst}$))
$\hat{Y}_{ij}$	estimated value of the dependent variable corresponding to temperature i and experiment j (initial specific reaction rate $mol_{C_2H_4}\ s^{-1}\ g^{-1}_{catalyst}$)
α	relative loss of mass of catalyst (–)
α_1	parameter of the hyperbolic law
α_2	parameter of the hyperbolic law
α_3	parameter of the hyperbolic law
$\chi^2(\nu)$	χ^2 distribution corresponding to ν degrees of freedom
μ_i	mean value of the dependent variable for sample i (initial specific reaction rate ($mol_{C_2H_4}\ s^{-1}\ g^{-1}_{catalyst}$) or specific production ($g_C\ g^{-1}{}_{catalyst}$))
ν	number of degrees of freedom

effect of the catalytic deactivation on the apparent rate constant was empirically correlated with a simple exponential equation. An understanding of catalyst deactivation phenomena during carbon nanotube synthesis is necessary in order to predict and to better control the production of carbon nanotubes at a large scale. It is therefore important to quantify the effect of catalyst deactivation on carbon nanotube growth.

The role of different gases in carbon nanotube or fiber formation, such as nitrogen and hydrogen, has also been investigated. The role of hydrogen in MWNT formation is also an open question. Some previous studies [20–22] have suggested that the role of hydrogen in carbon fiber formation is to limit or alleviate the poisoning of the metal catalysts by amorphous carbon. More recently, it has been suggested that an intermediate is involved in the formation of MWNTs and that hydrogen acts to reduce the rate of spontaneous dehydrogenation of the intermediate to form soot [23]. In the same way, it was recently suggested that hydrogen regulates spontaneous carbonization so that the formation of soot does not compete with the slower formation of nanotubes [24]. Indeed, soot is the least thermodynamically stable form of carbon structure, while fullerenes represent a more stable form of carbon than soot. When hydrogen is released spontaneously and rapidly, then soot is formed. The rearrangement of the carbon skeletal structure is easiest when a leaving species such as hydrogen is present. When that leaving species is removed too fast, then the carbon will not have enough time to rearrange itself into the most thermodynamically stable configuration before it gets locked into a local minimum free energy structure. The controlled elimination of hydrogen leads to the preferential formation of fullerenes, while the controlled elimination of hydrogen in the presence of a catalyst will form carbon nanotubes, because the catalyst will keep the cage from closing so that carbon nanotubes can be formed [25]. So the role of hydrogen is closely related to the deactivation of catalyst.

In the present work, the catalytic deactivation during carbon nanotube synthesis by the CCVD process is modeled and the influence of hydrogen on initial specific reaction rate, on catalytic deactivation and on specific relative productivity are studied and quantified. Ethylene is used as the carbon source and the used catalyst is a very active bimetallic cobalt–iron catalyst on a supported aluminum hydroxide.

2. Materials and methods

2.1. Experimental setup

The experimental setup consisted of a long quartz tube placed in a tubular furnace [26]. The feed gas composition and the total flow were adjusted by three electronic flow controllers, and total pressure in the reactor was equal to atmospheric pressure. By operating a bypass valve, the feed gas could be directed either toward the reactor or a bypass. The catalyst is placed into the hot part of the reactor. A mass spectrometer was placed at the exit of the device in order to measure continuously the composition of the exhaust gas. The carbon source was ethylene, balanced by helium and/or hydrogen. The used catalyst was an iron–cobalt catalyst supported on alumina [27]. It was synthesized by dry impregnation of a $Al(OH)_3$ (Acros) support whose particle size was smaller than 80 μm by a mixture of aqueous solutions of $Fe(NO_3)_3{\cdot}9H_2O$ (Acros) and $Co(NO_3)_2{\cdot}6H_2O$ (Acros) so as to get 10 wt.% of the metal on the support in order to obtain paste. Indeed, 50 g of $Al(OH)_3$ were added to a solution containing 12.9 g of $Fe(NO_3)_3{\cdot}9H_2O$ and 9.3 g of $Co(NO_3)_2{\cdot}6H_2O$, so as to get an atomic ratio Co/(Fe + Co) equal to 0.5. Then, the material was dried at 400 °C during 2 h until obtaining a powder which was ground into a fine powder.

2.2. Experimental design

The experimental design for a given temperature is presented in Fig. 1. It consisted of ethylene molar fractions ranging from 10% to 90%, balanced by hydrogen or by helium. For each experiment, the total gas flow rate was equal to $3.72 \times 10^{-3}\ mol\ s^{-1}$. Four temperatures were examined in that study: 600 °C, 650 °C, 675 °C and 700 °C. 22 replicates and 20 supplementary experimental conditions were also tested, corresponding to an ethylene molar fraction equal to 40%, balanced by an hydrogen molar fraction varying from

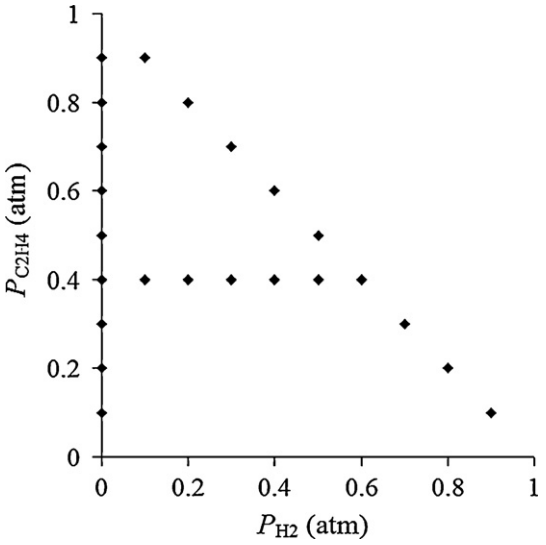

Fig. 1. Experimental design.

10% to 50% and helium to reach 100%. Those additional tests were performed in order to highlight the influence of hydrogen.

2.3. Determination of specific productivity and reaction rate

The initial specific reaction rate r_0 was determined from the slope of the tangent with the greatest slope of the cumulative hydrogen production curve, as shown in Fig. 2. Indeed, the hydrogen production is related to the ethylene consumption by the relation:

$$r_0 = -\frac{1}{(1-\alpha)m_{\text{catalyst}}}\frac{\mathrm{d}[C_2H_4]}{\mathrm{d}t} = \frac{1}{2(1-\alpha)m_{\text{catalyst}}}\frac{\mathrm{d}[H_2]}{\mathrm{d}t} \quad (1)$$

Where m_{catalyst} is the mass of catalyst, and α is the relative loss of mass of the catalyst due to moisture and solvent elimination when the catalyst is placed at high temperature. The relative loss of mass α was determined by weighing a sample of catalyst beforehand. After that, the sample was placed at 700 °C for 10 min under a helium flow. α was found to be equal to 23%. The experimental procedure leading to the cumulative hydrogen production curve for each experiment has been described in a previous paper [28]. For each experiment of the experimental design (Fig. 1), a mass of fresh catalyst of 0.5 g is weighed and placed into the reactor, and the total gas flow rate at the inlet of the reactor is equal to 6.1×10^{-3} m^3 s^{-1}.

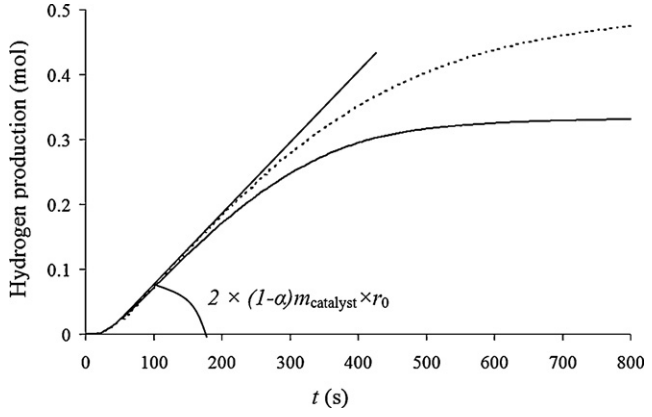

Fig. 2. Examples of cumulative hydrogen production curves as a function of time with hydrogen in the feed gas (dotted line) and without hydrogen in the feed gas (full line).

Table 1
Experimental initial specific reaction rates of carbon nanotube synthesis.

$P_{C_2H_4}$ (atm)	P_{H_2} (atm)	P_{He} (atm)	$r_0 \times 10^4$ ($\text{mol}_{C_2H_4}$ s^{-1} g^{-1}_{catalyst})			
			700 °C	675 °C	650 °C	600 °C
0.1	0	0.9	2.6	3.0	3.0	2.4
0.2	0	0.8	5.1	5.1	5.0	3.3
0.3	0	0.7	9.0	6.9	6.6	3.5
0.4	0	0.6	10.1	9.1	7.3	4.8
			10.1	10.2	7.9	4.9
			10.1	8.7	8.1	5.4
			10.7	10.0	7.6	
0.5	0	0.5	12.7	9.7	8.2	3.5
0.6	0	0.4	12.4	11.0	8.5	4.3
0.7	0	0.3	15.5	11.5	9.3	5.4
0.8	0	0.2	15.8	12.6	9.7	4.5
0.9	0	0.1	16.6	13.9	10.3	4.9
0.1	0.9	0	2.3	2.3	2.6	2.3
0.2	0.8	0	6.5	5.2	4.4	3.9
0.3	0.7	0	8.4	7.2	5.8	5.2
0.4	0.6	0	11.2	7.4	7.6	4.8
			10.4	7.8	7.3	4.5
			11.5	8.4	7.0	4.3
			10.3	7.7	8.2	
0.5	0.5	0	13.2	9.5	8.9	5.9
0.6	0.4	0	13.0	10.7	9.2	5.6
0.7	0.3	0	14.2	11.2	9.1	5.8
0.8	0.2	0	14.8	12.3	10.6	5.6
0.9	0.1	0	15.0	13.6	10.9	5.6
0.4	0.1	0.5	9.8	10.2	7.1	4.3
0.4	0.2	0.4	11.0	9.4	7.1	5.0
0.4	0.3	0.3	11.1	9.2	6.9	5.2
0.4	0.4	0.2	11.7	7.5	6.9	5.3
0.4	0.5	0.1	10.4	7.1	6.8	5.0

During the reaction, hydrogen production and ethylene consumption are recorded by a mass spectrometer. The reaction duration is equal to 15 min, time after which the reaction is completed. It has to be noted that as described in the literature [29], calculations showed that experiments were performed in the chemical regime, meaning that the measured reaction rates correspond to carbon nanotube growth.

The specific production Y was obtained by weighing the produced carbon nanotubes, the reaction being ended after 15 min for all experiments:

$$Y = \frac{m_{\text{CNTs}} - (1-\alpha)m_{\text{catalyst}}}{(1-\alpha)m_{\text{catalyst}}} \quad (2)$$

where m_{CNTs} is the mass of carbon nanotubes.

3. Results

3.1. Initial specific reaction rate

Initial specific reaction rates r_0 are given in Table 1.

3.2. Specific production of carbon nanotubes

The relative specific productions Y/Y_{max} at 700 °C are presented in Fig. 3. The relative specific production Y/Y_{max} corresponds to specific production Y divided by the maximum specific production Y_{max} at 700 °C. 700 °C is the temperature at which carbon nanotubes are industrially produced with ethylene as carbon source. Indeed, the specific production (Fig. 4) and the initial specific reaction rates (Fig. 5) are at their highest at 700 °C. In Fig. 4, Y/Y_{700} corresponds to specific production Y at the considered temperature for an ethylene partial pressure equal to 0.4 atm, divided by the production Y_{700} at 700 °C for an ethylene partial pressure equal to 0.4 atm. Beyond 700 °C, homogeneous phase decomposition of ethylene occurs and

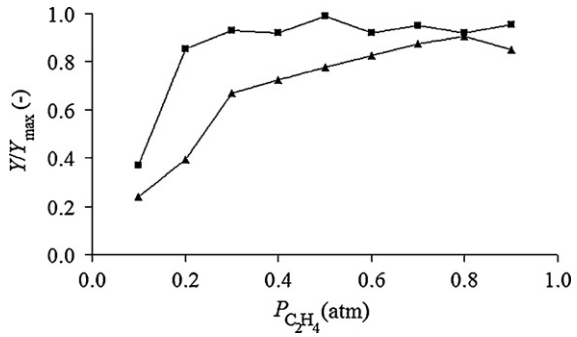

Fig. 3. Relative specific production of carbon nanotubes at 700 °C: —■—, with H_2; —▲—, with He.

soot is formed. Indeed, a hydrocarbon decomposes itself and forms soot when it is brought at a too high temperature, depending on the nature of the hydrocarbon [30]. For this reason, the reaction temperature was limited to 700 °C here.

4. Discussion

4.1. Influence of hydrogen on initial specific reaction rate

Fig. 6 highlights the influence of hydrogen partial pressure on the initial specific reaction rate of carbon nanotube synthesis at 700 °C for an ethylene partial pressure in the feed gas equal to 0.4 atm. It can be seen that hydrogen partial pressure does not influence the initial specific reaction rate. A statistical Student's *t*-test confirmed that observation; the statistical *t*-test allows determining whether two sets of data are really different or not [31]. Two sets of data were considered: the first sample consisted of the four experiments with an ethylene partial pressure equal to 0.4 atm balanced by helium, and the second sample consisted of the four experiments with an ethylene partial pressure equal to 0.4 atm balanced by hydrogen. The statistical *t*-test implies the determination of a t_{exp} variable calculated from experiments, which is defined by:

$$t_{exp}=\frac{\mu_1-\mu_2}{(((n_1-1)s_1^2+(n_2-1)s_2^2)/(n_1+n_2-1))\sqrt{(1/n_1)+(1/n_2)}} \quad (3)$$

where μ_1 and μ_2 are the mean values of samples 1 and 2 respectively, n_1 and n_2 are the size of samples 1 and 2 respectively, and s_1^2 and s_2^2 are the variance of samples 1 and 2 respectively. At 700 °C, the t_{exp} variable was found to be equal to 1.72, while the tabulated *t* variable for a number of degrees of freedom ν equal to 6 (=4 + 4 − 2) and with a significance level equal to 5% was found to be equal to 2.97. Because the tabulated *t* variable is greater than the experimental t_{exp} variable, it can be concluded, with regard to the initial specific reaction rate, that the sample corresponding to data with hydrogen belongs to the sample corresponding to data without hydrogen. So hydrogen partial pressure does not influence the initial specific reaction rate at 700 °C. A statistical *t*-test was also performed on experimental data at 675 °C, 650 °C and 600 °C, showing that the sample corresponding to data with hydrogen also belongs to the sample corresponding to data without hydrogen at 675 °C, 650 °C and 600 °C.

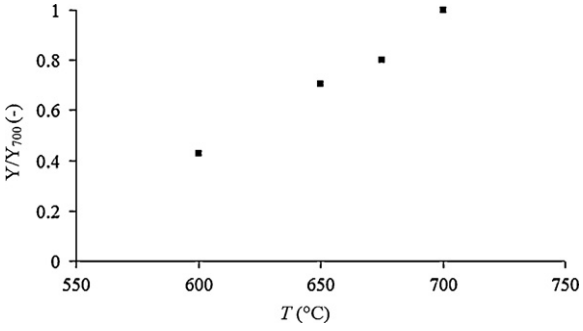

Fig. 4. Relative specific production of carbon nanotubes for an ethylene partial pressure equal to 0.4 atm with hydrogen.

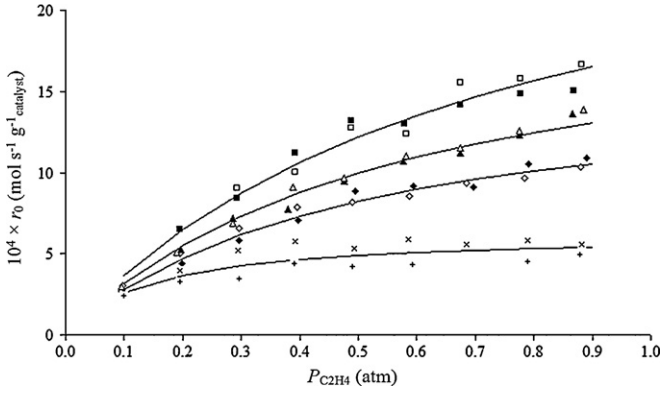

Fig. 5. Experimental initial specific reaction rates of carbon nanotube synthesis: ■, 700 °C with H_2; □, 700 °C with He; ▲, 675 °C with H_2; Δ, 675 °C with He; ♦, 650 °C with H_2; ◊, 650 °C with He; ×, 600 °C with H_2; +, 600 °C with He. The black curves correspond to model adjustment at 700 °C, 675 °C, 650 °C and 600 °C respectively.

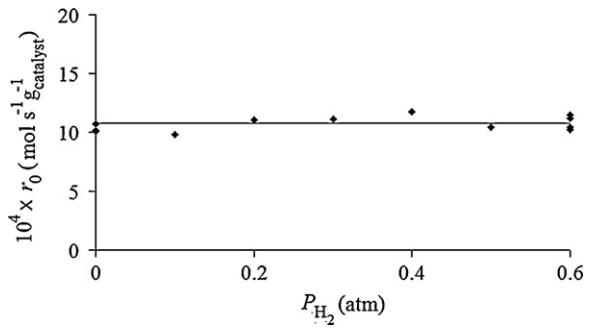

Fig. 6. Initial specific reaction rate at 700 °C as a function of hydrogen partial pressure for an ethylene partial pressure equal to 0.4 atm.

4.2. Kinetic study

A kinetic study was performed to describe the initial specific reaction rate of carbon nanotube synthesis. The software used for parameter estimation was derived from the NLPE program and the Gauss–Newton method was used to optimize parameters. A maximum likelihood formulation was adopted, thus minimizing the weighed sum of squares of the differences between calculated and measured initial specific reaction rates [32]. Initial specific reaction rates r_0 are shown in Fig. 5. Experimental data corresponding to a feed gas composed of ethylene balanced by hydrogen and/or helium treated as one whole set of data because hydrogen partial pressure does not influence the initial specific reaction rate. The best kinetic equation in agreement with experimental data on the basis of a statistical χ^2 test was to be [33]:

$$r_0=\frac{k\,K\,P_{C_2H_4}}{1+K\,P_{C_2H_4}}=\frac{A_2\exp(-E_2/RT)\exp(-\Delta H^\circ/RT)\exp(\Delta S^\circ/R)P_{C_2H_4}}{1+\exp(-\Delta H^\circ/RT)\exp(\Delta S^\circ/R)P_{C_2H_4}} \quad (4)$$

where $k, K, A, E_2, \Delta H^\circ, \Delta S^\circ$ are respectively the kinetic rate constant, the ethylene adsorption constant, the preexponential factor, the activation energy, the standard ethylene adsorption enthalpy and the standard ethylene adsorption entropy.

Adjusted curves are presented in Fig. 5 at 600 °C, 650 °C, 675 °C and 700 °C. They highlight the very good agreement between kinetic model and the experimental data. Only the mean value of each of two sets of 4 replicated points at an ethylene partial pressure equal to 0.4 atm is represented. Furthermore, the 15 points at an ethylene partial pressure equal to 0.4 atm with an increasing hydrogen partial pressure are not represented. However, adjustment was performed with all experimental data.

The statistical χ^2 test [31] performed on experimental data validate the kinetic model. Indeed, according to the χ^2 test, a model is validated when the calculated objective function S is smaller than the variable $\chi^2(\nu)$ for the corresponding number of degrees of freedom ν. The objective function S is defined as:

$$S = \sum_{i=1}^{3} \sum_{j=1}^{l_i} \left[\frac{(\hat{Y}_{ij} - Y_{ij})^2}{s_e^2} \right] \quad (5)$$

In Eq. (5), the subscript i corresponds to the temperature. Subscripts i = 1, 2, 3 and 4 correspond respectively to 600 °C, 650 °C, 675 °C and 700 °C. Subscript j refers to the number of experiments performed for each temperature. l_i is the number of experiments performed at each temperature and is equal to 29 at 650 °C, 675 °C and 700 °C and to 27 at 600 °C. $\hat{Y}_{ij}$, Y_{ij} and s_e^2 are respectively the estimated dependent variable (in this case, the initial specific reaction rate calculated by the kinetic model) corresponding to temperature i and experiment j, the experimental dependent variable corresponding to temperature i and experiment j (in this case, the experimental initial specific reaction rate r_0), and the experimental variance. The objective function S was found to be equal to 34.5. The number of degrees of freedom was equal to 88, corresponding to 114 measurements, minus 22 replicates, minus the 4 parameters of the kinetic model. So the variable $\chi^2(88)$ was equal to 67 with a probability of 95%. Therefore, the model can be considered to be validated according to the χ^2 test.

Eq. (4) corresponds to the following sequence of elementary steps, which consists of equilibrated adsorption of ethylene and of the irreversible surface ethylene decomposition as the rate-determining step [34]:

$$C_2H_4 + \underline{s} \overset{K}{\longleftrightarrow} \underline{C_2H_4 - s} \quad \text{equilibrated ethylene adsorption}$$

$$\underline{C_2H_4 - s} \overset{k_2}{\longrightarrow} \ldots\ldots\ldots \quad \text{irreversible ethylene decomposition}$$

other unspecified, kinetically non significant steps.

Activation energy E_2 was found to be equal to around $120 \pm 15\,\text{kJ mol}^{-1}$, standard adsorption enthalpy ΔH° to around $-120 \pm 20\,\text{kJ mol}^{-1}$, and standard adsorption entropy ΔS° to around $-120 \pm 20\,\text{J mol}^{-1}\,\text{K}^{-1}$. As a comparison with previous literature, reported activation energies for ethylene decomposition into carbon nanotubes and hydrogen vary between 100 kJ mol^{-1} and 180 kJ mol^{-1}, depending on the catalyst nature [28,34–37], while reported ethylene adsorption enthalpies with different catalyst vary from $-160\,\text{kJ mol}^{-1}$ to $-60\,\text{kJ mol}^{-1}$ [28,38,39]. Let us mention that ethylene adsorption enthalpy and entropy, ΔH° and ΔS°, must verify thermodynamic constraints. Indeed, adsorption is an exothermic process with decreasing entropy [33]:

$$\Delta H^\circ < 0$$
$$0 < -\Delta S^\circ < S^\circ_{C_2H_4} = 220\,\text{J mol}^{-1}\,\text{K}^{-1}$$

So values obtained are in agreement with those two constraints.

It has to be noted that a second mechanism, which implies a different sequence of elementary reaction steps based on a rate-determining active center, provides a rate expression that is mathematically identical [33,40] and that cannot, as a consequence, be statistically discriminated from Eq. (4):

$$r_0 = \frac{k_1 P_{C_2H_4}}{1 + (k_1/k_2) P_{C_2H_4}} = \frac{A_1 \exp(-E_1/RT) P_{C_2H_4}}{1 + (A_1/A_2)\exp(-(E_1 - E_2)/RT) P_{C_2H_4}} \quad (8)$$

where k_1, k_2, A_1, A_2, E_1 and E_2 are respectively the kinetic rate constant of elementary step 1, the kinetic rate constant of elementary step 2, the preexponential factor corresponding to elementary step 1, the preexponential factor corresponding to elementary step 2, the activation energy of elementary step 1, and the activation energy of elementary step 2. This mechanism assumes the irreversible adsorption of ethylene to an unspecified intermediate, followed by several unspecified steps leading to the formation of the most abundant reaction intermediate C–s [35]:

$$C_2H_4 + \underline{s} \overset{k_1}{\longrightarrow} \ldots\ldots\ldots\ldots \quad \text{irreversible ethylene adsorption}$$

other unspecified, kinetically non significant steps

$$\underline{C - s} \overset{k_2}{\longrightarrow} \ldots\ldots\ldots \quad \text{irreversible carbon diffusion}$$

The activation energy of irreversible ethylene adsorption E_1 was found to be equal to 0 kJ mol^{-1}, while activation energy of carbon diffusion E_2 was found to be equal to 120 kJ mol^{-1}. An activation energy of irreversible ethylene adsorption E_1 equal to 0 kJ mol^{-1} means that ethylene adsorption is not activated, which corresponds to most of adsorption processes. As a comparison with previous literature, Lee et al. [35], who proposed that the bulk diffusion of carbon plays a major role in determining the growth rate of carbon nanotubes, have found an activation energy equal to $130 \pm 15\,\text{kJ mol}^{-1}$ for carbon nanotube growth by thermal chemical vapor deposition using acetylene as carbon source and an iron catalyst.

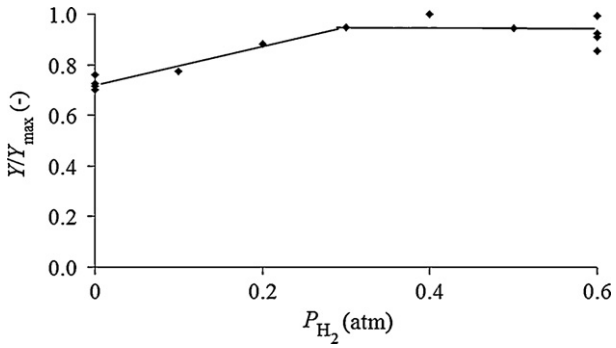

Fig. 7. Influence of hydrogen partial pressure on relative specific production of carbon nanotubes at 700 °C and for an ethylene partial pressure equal to 0.4 atm.

4.3. Specific production of carbon nanotubes

Relative specific productions Y/Y_{max} at 700 °C are highlighted in Fig. 3. It can be seen that the presence of hydrogen in the feed gas significantly improves the specific production of carbon nanotubes. This result can be explained by the role of hydrogen in amorphous carbon production. Indeed, amorphous carbon production avoids reactional gases to reach actives sites, and hydrogen reduces the rate of amorphous carbon deposition by dehydrogenation [24], leading to a decrease of the catalytic deactivation.

The influence of hydrogen on the specific production of carbon nanotubes produced at 700 °C for an ethylene partial pressure in the feed gas equal to 0.4 atm is highlighted in Fig. 7. An increase in specific production with increasing hydrogen partial pressure can be observed from 0 atm to 0.3 atm, and this confirms that the presence of hydrogen in the feed gas improves the specific production of carbon nanotubes. For greater hydrogen partial pressure, the specific production stays constant. A statistical Student t-test [31] was

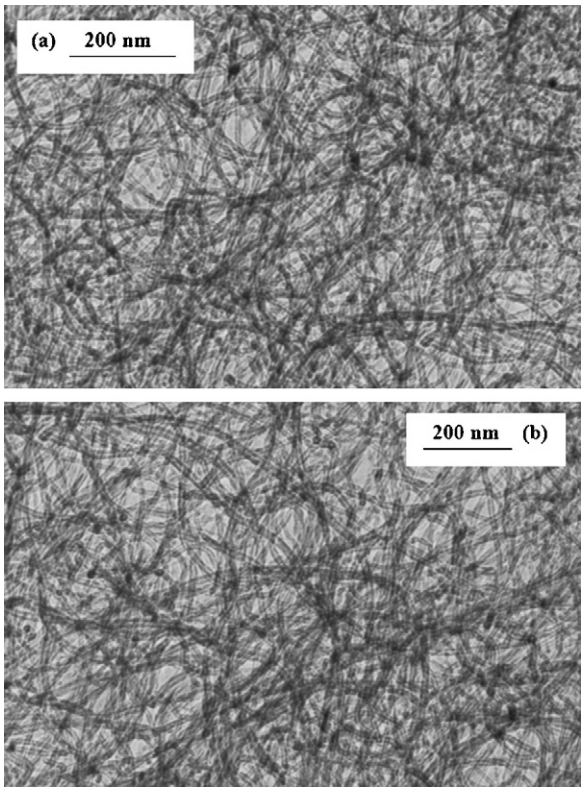

Fig. 8. TEM images of carbon nanotubes: (a) with hydrogen in the feed gas; (b) without hydrogen in the feed gas.

used to quantify the influence of hydrogen on specific productivity. The same two samples of data as for the initial specific reaction rate were considered: the first sample consisted of the four experiments with an ethylene partial pressure equal to 0.4 atm balanced by helium, and the second sample consisted of the four experiments with an ethylene partial pressure equal to 0.4 atm balanced by hydrogen. The t_{exp} variable calculated from the experiments was found to be equal to 6.33, while the tabulated t variable with a significance level equal to 5% was found to be equal to 2.97. Because the tabulated t variable is smaller than the experimental t_{exp} variable, it can be concluded that, with regard to the specific production of carbon nanotubes, the sample corresponding to data with hydrogen does not belong to the sample corresponding to data without hydrogen. So hydrogen partial pressure influences and improves the specific production of carbon nanotubes.

It has to be noted that the level of purity of produced carbon nanotubes cannot be quantified because the specific production is very high, due to the very high quality of the catalyst. TEM images performed on different samples do not shown any modification in carbon nanotube quality. The purity of carbon nanotubes is very high, whatever the experimental conditions. No soot is observed on TEM images, as shown in Fig. 8. Furthermore, no difference is qualitatively observed in the presence of hydrogen (Fig. 8a) or not (Fig. 8b).

4.4. Catalytic deactivation

Catalytic deactivation provides an explanation as to why hydrogen improves the specific production of carbon nanotubes even though the initial specific reaction rate does not vary when hydrogen is introduced into the reactor. It also allows this phenomenon to be quantified. Fig. 2 shows two examples of cumulative hydrogen production curve recorded by the mass spectrometer with and without hydrogen in the feed gas. It can be seen that reaction rate stays constant and maximal only for a while depending of operating conditions. After that time, reaction rate decreases and becomes progressively equal to zero. This is the catalytic deactivation. It can also be shown that the catalytic deactivation is slowed down in presence of hydrogen which plays a positive role on catalytic deactivation.

There are three categories into which the loss of catalytic activity can traditionally be divided: the sintering, the poisoning and the coking [41]. Concerning the present catalyst, an experiment was performed to determine the type of catalytic deactivation. It consists in burning the produced carbon nanotubes at 500 °C under air atmosphere during 6 h in order to recover the catalyst. Then, the recovered catalyst is used to produce carbon nanotubes again. The result is that the specific reaction rate and the specific productivity of carbon nanotubes are the same with the pristine catalyst and with the recovered catalyst. This means that the catalyst properties are not modified during the reaction and that there is no catalytic activity loss. So it can be concluded that the catalytic deactivation is due to coking and not to sintering or poisoning, because coking is the only type of deactivation which does not modify the number of active sites and the catalyst properties. This is in agreement with previous literature stating that the catalytic deactivation is due to the progressive accumulation on active sites of amorphous carbon by dehydrogenation [24].

A law commonly used to describe the phenomenon of catalytic deactivation by coking [33,41] corresponds to a decreasing hyperbolic law [33]:

$$\tilde{m} = \frac{1}{1 + \alpha_1 C_P} \tag{9}$$

where $\tilde{m}$ is the dimensionless active mass of catalyst and C_P is the amorphous carbon concentration. If one active site is obstructed by one amorphous carbon species, the amorphous carbon deposition order is equal to 1, and C_P can be expressed as:

$$C_P = \alpha_2 \exp[\alpha_3(t - a)] \tag{10}$$

The parameter a is necessary to quantify the latency time before the beginning of the catalytic deactivation and can be justified by the theory of free radical condensate proposed by Reilly and Whitten [23]. The free radical condensates are produced during carbon nanotube formation. As the tubes grow, the layer of radical condensates thickens. Because precursor soot is the condensate of free radicals, the progressive increase of the thickness of the radical condensate layer during carbon nanotube synthesis halts the carbon nanotube growth and soot preferentially form. So when the layer reaches a given thickness, carbon nanotube growth rate decreases and the deactivation by coking begins. This phenomenon is quantified by the parameter a.

So Eq. (9) becomes:

$$\tilde{m} = \frac{1}{1 + \alpha_1\alpha_2 \exp[\alpha_3(t - a)]} \tag{11}$$

After derivation, it can be written:

$$\frac{d\tilde{m}}{dt} = -\frac{\alpha_1\alpha_2\alpha_3}{(\exp[(-\alpha_3/2)(t - a)] + \alpha_1\alpha_2 \exp[(\alpha_3/2)(t - a)])^2} \tag{12}$$

By fixing $\alpha_1\alpha_2 = 1$, Eq. (12) becomes:

$$\frac{d\tilde{m}}{dt} = -\frac{\alpha_3}{\cosh^2[(\alpha_3/2)(t - a)]} \tag{13}$$

This expression corresponds to a sigmoid decreasing law. In this study, the modeled deactivation law has the same form and includes three parameters:

$$\frac{d\tilde{m}}{dt} = -\frac{b\,d}{\cosh^2(d(t - a))} \tag{14}$$

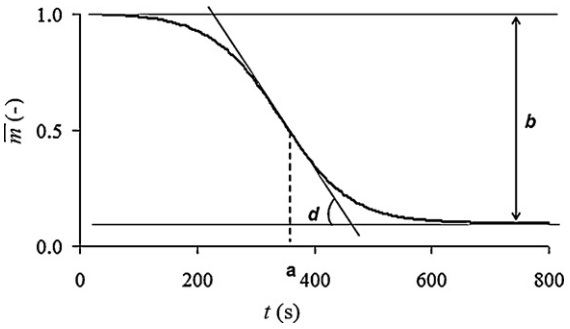

Fig. 9. Meaning of the parameters of the deactivation curve.

As shown in Fig. 9, parameter *a* corresponds to the abscission of the inflexion point of the sigmoid, parameter *b* quantifies the magnitude of the sigmoid decrease, and parameter *d* characterizes the slope of the curve at the inflexion point of the sigmoid. So, the greater the size of *a*, the more the deactivation is delayed, the lower the size of *b*, the more the deactivation is reduced, and lower the size of *d*, the more the deactivation is slowed down.

Estimates allow the determination of parameters *a*, *b* and *d* for each experimental condition. Parameter *a* is an increasing function of hydrogen partial pressure from 0 atm to 0.3 atm, then parameter *a* stays constant, as shown in Fig. 10a. This observation is in agreement with Fig. 7 showing that the specific productivity increases with hydrogen partial pressure from 0 atm to 0.3 atm, and then stays constant too. A statistical Student's *t*-test was used to quantify that observation [31]. The same two samples of data as for the initial specific reaction rate and specific production were considered: the first sample consisted of the four experiments with an ethylene partial pressure equal to 0.4 atm balanced by helium, and the second sample consisted of the four experiments with an ethylene partial pressure equal to 0.4 atm balanced by hydrogen. The t_{exp} variable calculated from the experiments was found to be equal to 5.36, while the tabulated *t* variable with a significance level equal to 5% was found to be equal to 2.97. Because the tabulated *t* variable is smaller than the experimental t_{exp} variable, it can be concluded that, with regard to parameter *a*, the sample corresponding to data with hydrogen does not belong to the sample corresponding to data without hydrogen. This means that hydrogen delays catalytic deactivation.

Parameter *b* does not vary with hydrogen partial pressure (Fig. 10b), which means that the magnitude of the deactivation does not vary in presence of hydrogen. Indeed, in each case, the relative mass of active catalyst is equal to 1 in the beginning of the reaction and becomes progressively equal to zero. That observation is quantified by a statistical Student's *t*-test. The t_{exp} variable calculated from the experiments was found to be equal to 1.56, while the tabulated *t* variable with a significance level equal to 5% was found to be greater and equal to 2.97.

Parameter *d* is a decreasing function of hydrogen partial pressure (Fig. 10c), which means that the presence of hydrogen slows down the catalytic deactivation. Indeed, a statistical Student's *t*-test [31] showed that the first sample of data consisted of the four experiments with an ethylene partial pressure equal to 0.4 atm balanced by helium, and the second sample of data consisted of the four experiments with an ethylene partial pressure equal to 0.4 atm balanced by hydrogen, were significantly different, because the t_{exp} variable was found to be equal to 8.10, which is greater than the tabulated *t* variable which was found to be equal to 2.97.

The influence of hydrogen on catalytic deactivation is highlighted in Fig. 11, corresponding to experiments performed with an ethylene partial pressure equal to 0.4 atm and with increasing hydrogen partial pressures, from 0 atm to 0.6 atm. It can be seen that

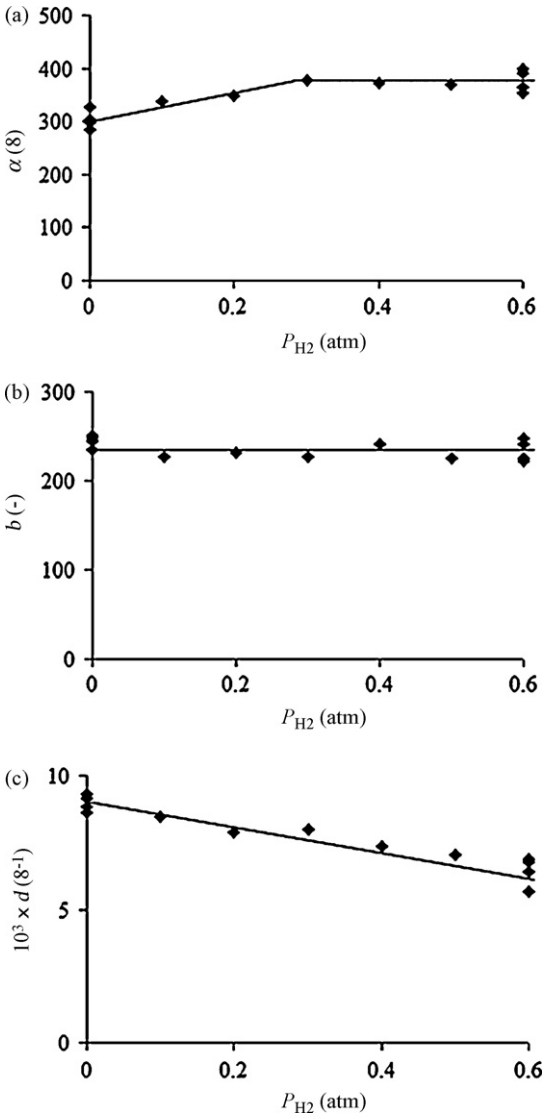

Fig. 10. Influence of hydrogen partial pressure on parameters of catalytic deactivation: (a) parameter *a*; (b) parameter *b*; (c) parameter *d*.

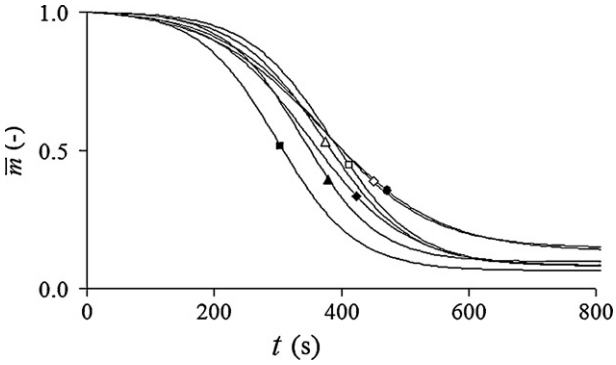

Fig. 11. Catalytic deactivation for experimental conditions corresponding to an ethylene partial pressure equal to 0.4 atm, balanced by a hydrogen partial pressure equal to: —■—, 0 atm; —▲—, 0.1 atm; —♦—, 0.2 atm; —□—, 0.3 atm; —Δ—, 0.4 atm; —◊—. 0.5 atm; —●—, 0.6 atm.

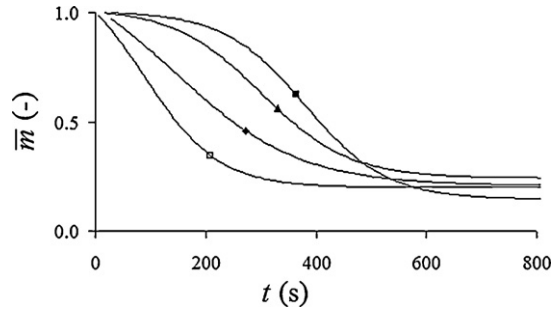

Fig. 12. Catalytic deactivation for experimental conditions corresponding to an ethylene partial pressure equal to 0.4 atm, balanced by hydrogen at: —■—, 700 °C; —♦—, 675 °C; —▲—, 650 °C; and —□—, 600 °C.

the presence of hydrogen delays and slows down the catalytic deactivation. Indeed, hydrogen avoids amorphous carbon formation by hydrocarbon dehydrogenation [24].

It has to be noted that other laws have been used to describe the catalytic deactivation, but the agreement between experimental and modeled deactivation curves was not satisfactory.

In a previous study [19], the catalytic deactivation during MWNT synthesis using xylene as precursor and iron particles as catalyst was correlated with a simple exponential equation. In the present work, the exponential equation cannot match to describe the catalytic deactivation. Indeed, the catalytic activity stays constant at its highest level for a moment depending on experimental conditions, and after that time the deactivation begins. This is the reason why the exponential equation and the hyperbolic equation with a parameter a equal to zero in Eq. (14), both corresponding to a catalyst whose deactivation begins instantaneously, cannot be used.

The catalytic deactivation was also modeled at 675 °C, 650 °C and 600 °C by a decreasing hyperbolic law. The deactivation curves for an ethylene partial pressure equal to 0.4 atm and a hydrogen partial pressure equal to 0.6 atm are compared in Fig. 12. It can be shown that the deactivation occurs earlier for smaller temperatures, meaning that the accumulation of amorphous carbon is slower at high temperature. The influence of temperature on initial specific reaction rate and on catalytic deactivation allows explaining why the specific productivity is smaller when the temperature decreases.

The deactivation of the catalyst studied in this work can be compared to the deactivation of other catalysts described elsewhere [13,14]. Fig. 13 compares the catalytic deactivation of the present catalyst and of one of the other catalysts. It can be said that the deactivation of the present catalyst is weaker. Fig. 13 highlights that the catalytic deactivation corresponding to the present catalyst is delayed, *i.e.* the catalyst stays active longer and the parameter a is greater. Indeed, the parameter a is equal to zero for other catalysts. The more rapid deactivation is due to the faster soot formation because active sites are quickly obstructed. It can be concluded that the catalyst studied in this work presents a great activity and can lead to great carbon nanotube productivity. Concerning the influence of hydrogen, it can be said that hydrogen delays and slows down catalytic deactivation, whatever the catalyst considered.

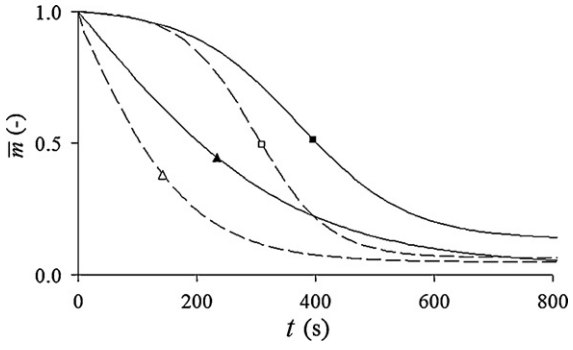

Fig. 13. Catalytic deactivation for experimental conditions corresponding to an ethylene partial pressure equal to 0.4 atm, balanced by hydrogen or helium: —▲—, other catalysts [13,14] with H_2; —Δ—, other catalysts [13,14] with He; —■—, present catalyst with H_2; —□—, present catalyst with He.

5. Conclusions

In the present work, the catalytic deactivation during MWNT synthesis by the CCVD process using an iron–cobalt catalyst supported on alumina and the influence of hydrogen on it were studied and quantified.

It was experimentally shown that reaction rate stays constant and maximal only for a while, and after that time, the catalyst deactivates and the catalytic activity becomes progressively equal to zero. The reason for this is the deposition of amorphous carbon on the catalytic surface leading to active site obstruction. This phenomenon was modeled by a phenomenological decreasing hyperbolic law whose parameters were estimated by parameter adjustments.

The presence of hydrogen was found to influence the catalytic deactivation during carbon nanotube synthesis. Indeed, for a given ethylene partial pressure, the catalytic deactivation was delayed and slowed down with increasing hydrogen partial pressure. The final level of catalytic activity was not influenced by hydrogen. The influence of hydrogen was quantified by parameters of the hyperbolic law. So the main role played by hydrogen is to delay and slow down the catalytic deactivation, confirming the results of previous qualitative studies stating that hydrogen promotes carbon nanotube production rather than soot production. As a consequence, the presence of hydrogen increases the specific production of carbon nanotubes because it maintains longer the catalytic activity at its highest level and does not influence the initial specific reaction rate.

Acknowledgments

S.L. Pirard is grateful to the National Funds for Scientific Research, Belgium (F.R.S.-FNRS) for a position of Postdoctoral Researcher. The authors also thank the Belgian Fonds pour la Recherche Fondamentale Collective (FRFC), the Région Wallonne – Direction Générale des Technologies, de la Recherche et de l'Énergie, the Ministère de la Communauté Française – Direction de la Recherche Scientifique, the Fonds de Bay and the Interuniversity Attraction Poles Program – Belgian State – Belgian Science Policy – P6/17 for their financial support. The involvement of the University of Liège in the Network of Excellence FAME of the European Union Sixth Framework program is also acknowledged.

References

[1] M. Monthioux, V.L. Kuznetsov, Carbon 44 (2006) 1621–1623.
[2] V.N. Popov, Mater. Sci. Eng. A 43 (2004) 61–102.
[3] A.M. Thayer, Chem. Eng. News 85 (2007) 29–35.
[4] B. Sigurg, K. Maziar, M. Volker, M. Leslaw, M. Christian, R. Reiner, W. Aurel, WO2007118668 (2007), EP2010701 A2.
[5] M. Bierdel, S. Buchholz, V. Michele, L. Mleczko, R. Rudolf, M. Voetz, A. Wolf, Phys. Status Solidi B 244 (2007) 3939–3943.
[6] P. Serp, R. Feurer, C. Vahlas, P. Kalck, WO03002456 (2003), US2004234445 A1.
[7] R. Philippe, P. Serp, P. Kalck, Y. Kihn, S. Bordère, et al., AIChE J. 55 (2009) 450–464.
[8] R. Philippe, A. Morançais, M. Corrias, B. Caussat, Y. Kihn, et al., Chem. Vap. Deposition 113 (2007) 447–457.
[9] J.P. Pirard, C. Bossuot, P. Kreit, WO2004069742 (2004), EP 1 594 802 B1.
[10] J.P. Pirard, Chem. Eng. News 86 (2008) 5.
[11] S.L. Pirard, C. Bossuot, J.P. Pirard, AIChE J. 55 (2009) 675–686.

[12] S.L. Pirard, G. Lumay, N. Vandewalle, J.P. Pirard, Chem. Eng. J. 146 (2009) 143–147.
[13] H. Kathyayini, I. Willems, A. Fonseca, J.B. Nagy, N. Nagaraju, Catal. Commun. 4 (2006) 140–147.
[14] K.Y. Tran, B. Heinrichs, J.F. Colomer, J.P. Pirard, S. Lambert, Appl. Catal. A 318 (2007) 63–69.
[15] R. Brukh, S. Mitra, Chem. Phys. Lett. 424 (2006) 126–132.
[16] N. Zhao, C. He, Z. Jiang, J. Li, Y. Li, Mater. Lett. 60 (2006) 159–163.
[17] R. Philippe, B. Caussat, A. Falqui, Y. Kihn, P. Kalck, J. Catal. 263 (2009) 345–358.
[18] J.F. Harris, Carbon 45 (2007) 229–239.
[19] K. Kuwana, H. Endo, K. Saito, D. Qian, D.R. Andrews, E.A. Grulke, Carbon 43 (2005) 253–260.
[20] K.L. Yang, R.T. Yang, Carbon 24 (1986) 687–693.
[21] Y. Nishiyama, Y. Tamai, J. Catal. 45 (1976) 1–5.
[22] M.S. Kim, N.M. Rodriguez, R.T.K. Baker, J. Catal. 131 (1991) 60–73.
[23] P.T.A. Reilly, W.B. Whitten, Carbon 44 (2006) 1653–1660.
[24] W.,W. Wasel, K. Kuwana, P.T.A. Reilly, K. Saito, Carbon 45 (2007) 833–838.
[25] Y. Ando, X. Zhao, T. Sugai, M. Kumar, Mater. Today 7 (2004) 22–29.
[26] J.F. Colomer, C. Stephan, S. Lefrant, G. Van Tendeloo, I. Willems, Z. Kónya, A. Fonseca, C. Laurent, J.B. Nagy, Chem. Phys. Lett. 317 (2000) 83–89.
[27] R.P. Silvy, F. Liégeois, B. Culot, S. Lambert, WO2006079186 (2006), EP 1827 680 B1.
[28] S.L. Pirard, S. Douven, C. Bossuot, G. Heyen, J.P. Pirard, Carbon 45 (2007) 1167–1175.
[29] C. Gommes, S. Blacher, C. Bossuot, P. Marchot, J.B. Nagy, J.P. Pirard, Carbon 42 (2004) 1473–1782.
[30] K. Saito, A.S. Gordon, F.A. Williams, W.F. Stickle, Combust. Sci. Technol. 80 (1991) 103–119.
[31] D.C. Montgomery, Design and Analysis of Experiments, Wiley, New York, 1997.
[32] P.E. Gill, W. Murray, M.H. Wright, Practical Optimization, Academic Press, California, 1981.
[33] M. Boudart, G. Djéja-Mariadassou, Kinetics of Heterogeneous Catalytic Reactions, Princeton University Press, New Jersey, 1984.
[34] K. Liu, C. Feng, Z. Chen, S. Fan, Carbon 43 (2005) 2850–2856.
[35] Y.T. Lee, J. Park, Y.S. Choi, H. Ryu, H.J. Lee, J. Phys. Chem. B 106 (2002) 7614–7618.
[36] R.D. Kamachali, Chem. Phys. 327 (2006) 138–434.
[37] L. Ni, K. Kuroda, L.P. Zhou, T. Kizuka, K. Ohta, K. Matsuishi, et al., Carbon 44 (2006) 2265–2272.
[38] S.L. Pirard, B. Heinrichs, G. Heyen, J.P. Pirard, Chem. Eng. J. 138 (2008) 367–378.
[39] J.M. Hill, J. Shen, R.M. Watwe, J.A. Dumesic, Langmuir 16 (2000) 2213–2219.
[40] S.L. Pirard, S. Douven, J.P. Pirard, Carbon 45 (2007) 3050–3052.
[41] H.S. Fogler, Elements of Chemical Reaction Engineering, fourth ed., Pearson Education, New Jersey, 2006.